

Variability and Predictability of Southeastern United States Summer Precipitation

HUI WANG^{1,4}, RONG FU², ARUN KUMAR¹, and WENHONG LI³

¹*Climate Prediction Center, NCEP/NWS/NOAA, Camp Springs, Maryland*

²*Department of Geological Sciences, University of Texas, Austin, Texas*

³*School of Earth and Atmospheric Sciences, Georgia Institute of Technology, Atlanta, Georgia*

⁴*Wyle Information Systems, McLean, Virginia*

Submitted to *Journal of Climate*
“USCLIVAR drought working group” special issue
December 5, 2008

Corresponding author address: Dr. Hui Wang, NOAA Climate Prediction Center,
5200 Auth Road, Camp Springs, MD 20746.
E-mail: hui.wang@noaa.gov

Abstract

The variability of summer precipitation in the Southeastern United States is examined in this study using 60-yr (1948–2007) rainfall data. The Southeast summer rainfall exhibits higher interannual variability with more intense summer droughts and anomalous wetness in the recent 30 years (1978–2007) than in the early 30 years (1948–77). Such intensification of summer rainfall variability is also reflected in the shift of daily rainfall probability distribution between the two periods. Changes in rainfall variability are also accompanied by a southward shift of the region of maximum zonal wind variability at the jet stream level in the late period.

The covariability between the Southeast summer precipitation and sea surface temperature (SST) is analyzed using the singular value decomposition (SVD) method. It is shown that the Southeast summer precipitation is coupled with the Atlantic and Pacific SST variations. However, the intensification of the Southeast summer rainfall variability is primarily associated with higher Atlantic SST variability in the recent three decades. An empirical model for predicting Southeast summer precipitation was developed based on the SVD analyses, which link the Southeast summer rainfall variability to the Atlantic zonal mode and the Atlantic SST warming trend, as well as the Pacific El Niño/La Niña mode. A cross validation of 60-yr hindcasts based on the observed SST suggests considerable potential predictability of the Southeast summer precipitation.

1. Introduction

The Southeastern United States is one of the fastest growing regions in the nation. Water supplies in this area are increasingly stressed especially during summer. The year-to-year fluctuations in summer rainfall over the Southeast thus have vital influence on regional hydrology, agriculture, and related industries. In the past three decades, summer droughts repeatedly struck the Southeast and had a devastating impact on this region socially and economically. For example, the 1986 Southeast summer drought caused billions of dollars of damage in agriculture (Bergman et al. 1986; Karl and Young 1987). The 2007 drought, the most recent one, ranked as the worst in 100 years and pushed water shortages to a crisis point.

The recurrence of severe droughts in recent decades raises a question as to whether the characteristics of rainfall in the Southeast have changed. If so, what might have caused such a change? This study aims to characterize the shift in summer rainfall variability in the Southeast and to explore the link between the shift in rainfall variability and the variability of sea surface temperature (SST).

Compared to warm season rainfall in the Great Plains (e.g., Namias 1983; Chang and Wallace 1987; Laird et al. 1996) and the North American monsoon region (Higgins et al. 2003), the variability of Southeast summer precipitation has received less attention in previous studies. In terms of seasonal mean precipitation and its variability, however, summer rainfall in the Southeast constitutes an important part of warm season precipitation over the continental United States. As shown in Fig. 1a, summer U.S. precipitation is characterized by abundant rainfall ($> 4 \text{ mm day}^{-1}$) along the Southeast coast. The seasonal mean precipitation increases from less than 1 mm day^{-1} in the

southwest to over 5 mm day^{-1} in the southeast corner. In the central and eastern United States precipitation is generally above 3 mm day^{-1} . Figure 1b shows the variance of summer precipitation. High interannual variability is found in both central and southeastern United States. A better understanding of the Southeast summer precipitation variability is thus essential for an improved prediction of U.S. warm season rainfall.

Recent observational and modeling studies indicate that droughts over the Southeastern United States are less persistent (Mo and Schemm 2008) and they are primarily controlled by internal atmospheric variability (Seager et al. 2008). The results suggest a low predictability of the Southeast summer precipitation. In this study, we will present observational evidence that the intensification of Southeast summer rainfall variability, as well as more severe droughts in recent decades, are closely tied to the variation of tropical Atlantic SST. The strong covariability between the rainfall and SST also suggests potential predictability of Southeast summer precipitation based on the tropical SST.

2. Data and method

The data used in this study consist of precipitation, atmospheric wind field, and SST from 1948 to 2007. Summer seasonal means are obtained by averaging together the monthly means of June, July, and August (JJA). An anomaly is defined as the deviation of a seasonal mean from its 60-yr long-term climatology. The U.S. precipitation data are taken from the National Oceanic and Atmospheric Administration (NOAA) Climate Prediction Center (CPC) U.S. Unified Precipitation for 1948–98 and from the realtime U.S. Daily Precipitation Analysis for 1999–2007. Both datasets are on a $0.25^\circ \times 0.25^\circ$

(lat × lon) grid. The atmospheric winds are the National Centers for Environmental Prediction – National Center for Atmospheric Research (NCEP–NACR) Reanalysis product (Kalnay et al. 1996) on a $2.5^\circ \times 2.5^\circ$ grid. The SSTs are the NOAA Extended Reconstructed SST (ERSST v3; Smith et al. 2008) with a $2^\circ \times 2^\circ$ (lat × lon) resolution.

The relationship between the Southeast summer precipitation and SST is examined by using the singular value decomposition (SVD; Bretherton et al. 1992). This statistical technique identifies pairs of spatial patterns with the maximum temporal covariance between precipitation and SST (e.g., Ting and Wang 1997; Wang and Ting 2000). Linear and multiple linear regressions are employed to composite and reconstruct anomalous atmospheric circulation and precipitation based on one or multiple base time series. The significance of the statistical results is estimated by the Monte Carlo technique (e.g., Wilks 1995).

3. Variability of Southeast summer rainfall

To describe the variability of summer rainfalls in the Southeast, a precipitation index is constructed by averaging June, July and August monthly mean precipitation anomalies in an area from 76°W to 91°W and from 25°N to 36.5°N . The area covers seven southeastern states, including Alabama, Florida, Georgia, Mississippi, North Carolina, South Carolina, and Tennessee. The normalized index time series for the 60 years (1948–2007) is shown in Fig. 2a, with one standard deviation corresponding to 0.64 mm day^{-1} . The precipitation index displays higher interannual variability with more wet and dry extremes in the second half of the period (1978–2008). In the first 30 years (1948–77), there were only two wet and two dry summers with rainfall anomalies

exceeding one standard deviation. In the second 30 years, however, there were six wet and five dry summers with rainfall anomalies greater than one standard deviation. The summer precipitation in the second half of the period contributes to the total rainfall variance by 68%, in contrast to 32% in the first 30 years.

To quantify characteristics of droughts shown in Figures 2b and 2c are the corresponding time series of the standardized precipitation index (SPI; McKee et al. 1993) on 3-month and 9-month time scales, respectively. Consistent with the precipitation index, the two SPI time series also indicate much more extremely wet and dry summers on both short and longer time scales existed in the latter period than in the early period. Since the 60-yr rainfall data consist of measurements from both pre- and post-satellite and radar eras, the results presented in Fig. 2 may be sensitive to the changes of the techniques in measuring precipitation over time. To examine this potential impact, a similar precipitation index is constructed using rain gauge observations from 154 stations that are available in the U.S. Historical Climatology Network (Williams et al. 2007) with a relatively homogeneous distribution over the seven Southeast states. The precipitation index based on these station data (not shown) is very similar to that in Fig. 2a with higher rainfall variability in the recent three decades confirming that the Southeast summer rainfall variability has been intensified since the late 1970s.

The relationship between the change in the interannual variability of summer precipitation and the frequency and intensity of daily rainfalls is examined by classifying the daily rain rates of summer extremes and then comparing them to corresponding long-term mean values. Figure 3 shows the mean distribution of summer days with different daily rain rates for the entire 60 years together with the composites of the five wettest and

five driest summers in the 1948–77 and 1978–2007 periods, respectively. A day with precipitation less than 0.1 mm day^{-1} is defined as a non-rainy day. For rainy days rainfall intensities are divided into three classes, namely, $0.1\sim 1 \text{ mm day}^{-1}$, $1\sim 10 \text{ mm day}^{-1}$, and greater than 10 mm day^{-1} . In each rain rate class, the number of days between June and August with the appropriate rain rate is averaged over all the grid points in the Southeast domain ($25^{\circ}\text{--}36.5^{\circ}\text{N}$, $76^{\circ}\text{--}91^{\circ}\text{W}$) for the years of interest.

The composite results indicate that over the 60 years 35% of the summer days are non-rainy days. The distributions of summer days in the three rain rate classes are 18% ($0.1\sim 1 \text{ mm day}^{-1}$), 34% ($1\sim 10 \text{ mm day}^{-1}$), and 13% ($> 10 \text{ mm day}^{-1}$), respectively. The statistics for both 30-yr periods (not shown) are similar to those of the 60 years. However, the rain rate distribution changes considerably in the extremely dry and wet summers, especially during the second 30-yr period. As shown in Fig. 3, the number of non-rainy days increases (decreases) in dry (wet) summers. The percentage of non-rainy days varies 9% between the wet and dry summers in the earlier period and increases to 18% in the second period. During the extreme summers, the number of rainy days with small rain rates ($0.1\sim 1 \text{ mm day}^{-1}$) does not differ much from the long-term mean. However, the number of days with larger rain rates ($> 1 \text{ mm day}^{-1}$) is coherently higher in wet summers and lower in dry summers. The difference in the rain rate distribution between wet and dry summers is greater in the second half of the period than in the first half.

Figure 3 suggests that a larger shift of rainfall probability distribution between wet and dry summers in the second 30 years contribute to the observed higher summer precipitation variability. The changes in the rain rate distribution between the two 30-yr

periods are above the 10% significance level for dry composites except for the heavy rain rate class ($> 10 \text{ mm day}^{-1}$) and above the 15% significance level for wet composites except for the light rain rate class ($0.1\sim 1 \text{ mm day}^{-1}$), as estimated by the Monte Carlo tests with the Bootstrap resampling technique (e.g., Wilks 1995).

As an important part of the continental-scale warm season rainfall in the United States, Southeast summer precipitation is fundamentally controlled by the large-scale atmospheric circulation (Liu et al. 1998). Figure 4 shows both upper- and low-level circulation anomalies associated Southeast summer droughts obtained based on linear regressions of the 60-yr data vs. the Southeast summer precipitation index (Fig. 2a). The drought-related circulation is dominated by positive height anomalies over the central United States and negative zonal wind anomalies over the southern states (Fig. 4a). The upper-level jet stream thus shifts towards the north. In the low level, the anticyclonic circulation enhances the Great Plains' low-level jet and moisture transport from the Gulf of Mexico to the Midwest, and also causes a deficit of moisture flux from the Gulf to the Southeast. The circulation pattern and associated low-level divergence field are consistent with dry conditions in the Southeast and wet conditions in the Midwest. The out-of-phase relationship between precipitation anomalies in the Southeast and the Midwest is one of the major patterns of warm season rainfall in the United States and has been identified in previous studies (e.g., Ting and Wang 1997). In the summers of 1993 and 2007, for example, while the Midwest suffered from devastating floods, the Southeast experienced severe droughts.

The change in the Southeast summer rainfall variability is also closely related to changes in the atmospheric circulation variability. Figure 5 shows the 200-hPa zonal

wind variance for the two 30-yr periods. There is a significant southward shift of the center of maximum zonal wind variance from 45°N in the early period to 40°N in the late period. The zonal wind variability at the jet stream level is also generally increased over the southern states in the second 30 years, where the zonal winds significantly correlate with the Southeast precipitation (Fig 4a). It is thus dynamically consistent with the intensification of Southeast summer rainfall variability.

4. Covariability with SST

To explore possible connection of the Southeast precipitation to Pacific and Atlantic SST, two SVD analyses were performed by analyzing the covariance matrices of summer season U.S. rainfall and SST from each ocean basin. Table 1 lists the statistics for the first SVD mode with the Pacific SST and two leading modes with the Atlantic SST, including the percentage of squared covariance explained by each mode, the temporal correlation between each pair of expansion coefficients, and the variance in individual fields that are explained by each mode. The spatial patterns of these SVD modes are shown in Fig. 6 with homogeneous correlation maps (Wallace et al. 1992).

For the Pacific SST, the first SVD mode is characterized by the El Niño SST pattern, with the large positive correlations in the eastern and central equatorial Pacific, as well as along the west coast of North America, and negative correlations in the central North Pacific (Fig. 6a). The corresponding precipitation (Fig. 6b) displays wet conditions in the Northern Plains and the Midwest and dry conditions in the Southeast. This is the canonical summer precipitation pattern associated with El Niño – Southern Oscillation (ENSO), also identified by the same SVD analysis in Ting and Wang (1997).

This mode explains 40% of the squared covariance between the Pacific SST and U.S. precipitation. The rainfall pattern itself explains 7% of the total summer precipitation variance over the United States.

For the Atlantic SST, the first SVD explains 35% of the squared covariance between the Atlantic SST and U.S. precipitation. The SST pattern (Fig. 6c) features warm SST anomalies across the tropical and North Atlantic. This Atlantic warming is also correlated with SST anomalies in the Indo-Pacific warm pool, the region experiencing significant warming in the past 60 years (e.g., Wang and Mehta 2008). The first mode of precipitation, which explains 10% of the total summer U.S. precipitation variance, has a well-defined pattern with the positive correlations in the Southeast and the Southern Plains (Fig. 6d). Associated with the Atlantic warming, summer precipitation in the Gulf States, especially Texas, is above normal.

The second SVD mode explains 19% of the squared covariance. The SST pattern (Fig. 6e) displays a band of positive correlations centered at the equator, which closely resembles the Atlantic zonal mode (Zebiak, 1993). Additionally, a zonal band of positive correlations is found in the North Atlantic centered at 45°N. The precipitation pattern (Fig. 6f) shows coherent negative correlations in the Southeast, where the summer precipitation index (Fig. 2a) is constructed, and positive correlations in the Midwest. This mode accounts for 9% of the precipitation variance, which is close to the Atlantic warming mode and higher than the ENSO mode. When the Atlantic zonal mode is in its warm phase, there is a tendency of decreasing summer rainfall across the Southeast.

The time series of the expansion coefficients for the three SVD modes are shown in Fig. 7. The temporal correlation between the Pacific SST and associated precipitation

time series (Fig. 7a) is 0.63, highest among the three modes (Table 1). The SST time series (Fig 7a, dark bars) displays large positive and negative fluctuations in El Niño (e.g., 1957, 65, 72, 83, 87, 92, 93 and 97) and La Niña (e.g., 1950, 55, 64, 70, 71, 73, 75, 88, and 99) years, respectively. A trend toward warmer SST starting in the late 1970s is also discernible, which was reported by Trenberth and Hurrell (1994). The precipitation time series (Fig. 7a, light bars) exhibits coherent fluctuations with the ENSO SST, indicating a strong association between the rainfall pattern in Fig. 6b and the El Niño/La Niña SST variation. The precipitation time series also shows a similar trend, corresponding to wetter conditions in the Northern Plains and the Midwest, and drier conditions in the Southeast in more recent years.

The correlation between the pair of the first SVD mode time series of Atlantic SST and U.S. precipitation (Fig. 7b) is 0.60. Both SST and precipitation are dominated by an upward trend, with the shift of SST anomalies from a cold phase to a warm phase in the early 1980s. This coincides with the phase change of global mean SST anomaly around the same time (IPCC, 2007). The correlation between the two time series for mode 2 (Fig. 7c) is 0.58. In recent years, the SST and precipitation fluctuations are relatively larger, indicating increased variability of the Atlantic zonal mode and the coupled rainfall pattern (Fig. 6f), which has high loadings in the Southeast.

Table 2 lists the contributions of the two 30-yr periods, respectively, to the total variance of each SVD time series over the entire 60 years. The increase of the Atlantic SST variability in the recent 30 years in both the warming trend and the zonal mode is consistent with the increase of the precipitation variability in the corresponding modes over the same period. Both SVD modes have strong loadings over the Southeast in the

precipitation field (Fig. 6). Therefore, the intensification of the Southeast summer rainfall variability is strongly coupled with the higher Atlantic SST variability in the last three decades.

In addition, the higher Atlantic SST variability in the late period also accounts for the change of the atmospheric circulation variability between the two 30 years (Fig. 5). Figure 8 shows the 200-hPa zonal wind variance associated the Pacific ENSO mode, the SST warming trend, and the Atlantic zonal mode, respectively, over the two 30-yr periods. They are reconstructed with linear regressions vs. the SST time series of each SVD mode. There are significant increases in the upper-level zonal wind variability over the central and southern United States in the second 30 years associated with the two Atlantic SST modes (Figs. 8d,8f). These changes contribute to the observed southward shift of the region of maximum zonal wind variability and the larger zonal wind variability over the southern states in the late period (Fig. 5).

The SVD analyses capture the relation of the U.S. precipitation to the Pacific and Atlantic SST. The correlation of the ENSO SST time series (Fig. 7a) with the time series of the two Atlantic SST modes (Figs. 7b,7c) are 0.13 and -0.04 , respectively. This indicates that the two Atlantic SST modes are largely independent of the ENSO mode. The correlation between the time series of the two Atlantic SST modes is 0.44. However, when the linear trend is removed from the time series of the first SST mode, their correlation reduces to 0.27, suggesting that the interannual variability of the two Atlantic modes is relatively independent. Although all three SVD precipitation patterns (Fig. 6, right) have high loadings in the Southeast, they are distinctive in the centers of action. The rainfall patterns coupled with the ENSO SST and the SST warming trend (Figs. 6b,6f)

more emphasize the rainfall variability in the eastern and western parts of the domain, respectively, whereas the rainfall pattern coupled with the Atlantic zonal mode (Fig. 6d) focuses on the central part of the Southeast.

How the SST-coupled precipitation patterns contribute to the Southeast rainfall variability is assessed by reconstructing the Southeast precipitation index based on multiple linear regressions against the three SVD precipitation time series. As shown in Fig. 9, the reconstructed total rainfall anomalies well reproduce the observed precipitation variation with a correlation of $R=0.92$. Among the three SVD modes, the Atlantic zonal mode-related precipitation change contributes most to the Southeast rainfall variability ($R=0.87$). The warming trend also has a significant contribution ($R=0.63$), whereas the ENSO mode has contributed less ($R=0.39$). Note that the threshold for the correlation coefficients exceeding the 1% significance level is 0.29 based on the Monte Carol tests. In the 15 wet and dry summers with the precipitation index exceeding 1 standard deviation (Fig. 2a, black bars), the ENSO mode only dominates the 1993 drought. The rest 14 summers are dominated by the Atlantic zonal mode. On average, for the 15 summers, the precipitation pattern coupled with the Atlantic zonal mode accounts for 70% of the reconstructed Southeast rainfall anomalies, while those coupled with the warming trend and the ENSO mode account for 22% and 8%, respectively.

5. Predictability of the Southeast summer precipitation

The results presented in Figs. 6, 7, and 9 suggest that the variability of the Southeast summer precipitation is strongly linked to the Atlantic and Pacific SST. The

SST thus may have potential predictive value for the Southeast summer precipitation. Given Atlantic and Pacific SST patterns, the Southeast precipitation can be predicted based on the relationship depicted by the SVD analyses (Figs. 6 and 7). The empirical forecast system involves three steps. First, seasonal mean SSTs of a target summer, for example, taken from climate model forecasts, are projected onto the SVD SST patterns (Fig. 6) to obtain the SST projection coefficients. The corresponding precipitation projection coefficients are then derived based on the SVD SST–precipitation relationship (Fig. 7) and a linear regression. Finally, precipitation anomalies are predicted with multiple linear regression coefficients of historical rainfall data vs. the three SVD precipitation time series, multiplied by the precipitation projection coefficients for the target summer. The proposed forecast method is similar to Wang et al. (1999).

The predictability of the Southeast summer precipitation is evaluated by a cross validation of the hindcasts of summer rainfall for the past 60 years (JJA, 1948–2007). Since no hindcasts of SST for the past 60 summers are available, the hindcasts of the 60-yr summer precipitation were made based on the observed JJA SST. Therefore, we measure the *potential predictability* of summer precipitation with a perfect seasonal SST forecast. Figure 10 shows the anomaly correlation between the hindcasts and observations of summer U.S. precipitation. Considerable forecast skill is found in the Northern Plains and the Southeast. The former is primarily contributed by the Pacific ENSO mode, whereas the latter is mainly contributed by the Atlantic zonal mode and the warming trend. Similar SVD analyses may also be performed using JJA U.S. precipitation and March, April and May (MAM) SST. Then the empirical forecast system can be applied to predicting summer U.S. precipitation based on the observed

MAM SST and the SST–precipitation relationship obtained from the lagged SVD analyses.

6. Conclusions and discussions

Our analysis of the 60-yr rainfall data reveals that the interannual anomalies of summer precipitation in the Southeastern United States have been intensified in recent three decades (1978–2007) compared to the earlier three decades (1948–77), leading to stronger summer droughts and anomalous wetness. Such intensification of summer rainfall variability is also reflected in the shift of daily rainfall probability distribution between the two 30 years. There is a larger decrease of rainfall frequency and intensity in dry summers and increase of rainfall frequency and intensity in wet summers in the late period. It is also accompanied by a southward shift of the region of maximum zonal wind variability at the jet stream level.

The SVD analysis is applied to the 60-yr summer U.S. precipitation with the Pacific SST and the Atlantic SST, separately. Three precipitation patterns are objectively identified, all of which have significant loadings in the Southeast and are coupled with the Pacific ENSO mode, the Atlantic warming trend and the Atlantic zonal mode, respectively. The two Atlantic SST modes show higher interannual variability in the recent 30 years, consistent with the intensification the Southeast summer rainfall variability, and also account for the observed southward shift of the upper-level maximum zonal wind variability in the late period. It is demonstrated that the precipitation pattern coupled with the Atlantic zonal mode contributes most to the Southeast summer precipitation variability. An empirical model for predicting U.S.

summer precipitation was developed based on the relationships between the Pacific/Atlantic SST and U.S. precipitation depicted by the SVD analyses. A cross validation of 60-year hindcasts based on the observed SST suggests a potentially considerable predictability of the Southeast summer precipitation.

The intensification of the Southeast summer precipitation variability closely ties to the higher Atlantic SST variability in the recent three decades. However, the question of what causes the increase of the Atlantic SST variability and the Southeast rainfall variability, especially in terms of natural variability vs. anthropogenic forcing, still remains unanswered. Previous study based on tree ring records has suggested that decade-long extreme droughts may have been a prominent feature in the Southeastern United States over the past 1000 years (Stahle and Cleaveland 1992). On the other hand the 1978–2007 period corresponds with an overall warming of tropical SST globally and the pattern of the SST warming in the Atlantic resembles those of the linear warming trend observed and simulated by climate models with increasing atmospheric CO₂ during the last few decades (Hegerl et al. 2007). Thus, both the increase of the Atlantic SST and the Southeast precipitation could be a manifestation of global warming in the observational record. In fact, the Intergovernmental Panel on Climate Change (IPCC; 2007) projected that in the 21st century increasing heavy rains and extreme droughts will be one of the consequences of global warming. In the extratropics, increasing precipitation intensity is mainly caused by increased water vapor in warmer air, as well as by changes in atmospheric circulation (Meehl et al. 2005). A global coupled climate model also shows that the increase in greenhouse gases would produce more frequent and more intense heat waves in the southern United States (Meehl and Tebaldi 2004), which

could lead to higher rates of evaporation, drying out the soil, and increasing the probability of severe droughts. Although it is difficult to directly assess the effect of global warming on the intensification of summer precipitation variability in the Southeast and the increase of the Atlantic SST variability in this study, the shift of the rainfall variability is consistent with what is expected in future, and could thereby already have been affected by warming trends. Further modeling and diagnostic studies are necessary to understand the physics and the impact of the global warming on the changes in the Atlantic SST and Southeast precipitation variability.

Acknowledgments. This work was supported by the NOAA Climate Prediction Program for the Americas (CPPA) Grant GC06–246. The NOAA ERSST v3 data and NCEP – NCAR Reanalysis data are provided by the NOAA/OAR/ESRL PSD, Boulder, Colorado, USA, from their web site at <http://www.cdc.noaa.gov>.

REFERENCES

- Bergman, K. H., C. F. Ropelewski, and M. S. Halpert, 1986: The record southeast drought of 1986. *Weatherwise*, **39**, 262–266.
- Bretherton, C. S., C. Smith, and J. M. Wallace, 1992: An intercomparison of methods for finding coupled pattern in climate data. *J. Climate*, **5**, 541–560.
- Chang, F. C., and J. M. Wallace, 1987: Meteorological conditions during heat waves and droughts in the United States Great Plains. *Mon. Wea. Rev.*, **115**, 1253 – 1269.
- Hegerl, G. C., and Co-authors, 2007: Understanding and Attributing Climate Change. *Climate Change 2007: The Physical Science Basis. Contribution of Working*

- Group I to the Fourth Assessment Report of the Intergovernmental Panel on Climate Change*. Solomon, S., D. Qin, M. Manning, Z. Chen, M. Marquis, K.B. Averyt, M. Tignor and H.L. Miller (eds.). Cambridge University Press, Cambridge, United Kingdom and New York, NY, USA.
- Higgins, R. W., and Coauthors, 2003: Progress in Pan American CLIVAR: The North American Monsoon System. *Atmosfera*, **16**, 29-65.
- Intergovernmental Panel on Climate Change (IPCC), 2007: Climate Change 2007: Synthesis report. *Summary for Policymakers*, pp 22.
- Kalnay, E., and Coauthors, 1996: The NCEP–NCAR 40-Year Reanalysis Project. *Bull. Amer. Meteor. Soc.*, **77**, 437–471.
- Karl, T. R., and P. J. Young, 1987: The 1986 Southeast drought in historical perspective. *Bull. Amer. Meteor. Soc.*, **68**, 773–778.
- Laird, K. R., S. C. Fritz, K. A. Maasch, and B. F. Cumming, 1996: Great drought intensity and frequency before AD 1200 in the Northern Great Plains, USA. *Nature*, **384**, 552–554.
- Liu, A. Z., M. Ting, and H. Wang, 1998: Maintenance of circulation anomalies during the 1988 drought and 1993 floods over the United States. *J. Atmos. Sci.*, **55**, 2810–2832.
- McKee, T. B., N. J. Doesken, and J. Kleist, 1993: The relationship of drought frequency and duration to time scales. Preprints, *Eighth Conf. on Applied Climatology*, Anaheim, CA, Amer. Meteor. Soc., 179–184.

- Meehl, G. A., J. M. Arblaster, and C. Tebaldi, 2005: Understanding future patterns of increased precipitation intensity in climate model simulations. *Geophys. Res. Lett.*, **32**, L18719, doi:10.1029/2005GL023680.
- Meehl, G. A., and C. Tebaldi, 2004: More intense, more frequent, and longer lasting heat waves in the 21st Century. *Science*, **305**, 994–997.
- Mo, K. C., and J. E. Schemm, 2008: Drought and persistent wet spells over the United States and Mexico. *J. Climate*, **21**, 980–994.
- Namias, J., 1983: Some causes of United States drought. *J. Climate Appl. Meteor.*, **22**, 30–39.
- Seager, R., A. Tzanova, and J. Nakamura, 2008: Drought in the Southeastern United States: Causes, variability over the last millennium and the potential for future hydroclimate change. *J. Climate*, submitted.
- Smith, T. M., R. W. Reynolds, T. C. Peterson, and J. Lawrimore, 2008: Improvements to NOAA's historical merged land-ocean surface temperature analysis (1880–2006). *J. Climate*, in press.
- Stahle, D. W., and M. K. Cleaveland, 1992: Reconstruction and analysis of spring rainfall over the southeastern U.S. for the past 1000 years. *Bull. Amer. Meteor. Soc.*, **73**, 1947–1961.
- Ting, M., and H. Wang, 1997: Summertime U.S. precipitation variability and its relation to Pacific sea surface temperature. *J. Climate*, **10**, 1853–1873.
- Trenberth, K. E., and J. Hurrell, 1994: Decadal atmosphere-ocean variations in the Pacific. *Climate Dyn.*, **9**, 303–319.

- Wallace, J. M., C. Smith, and C. S. Bretherton, 1992: Singular value decomposition of wintertime sea surface temperature and 500-mb height anomalies. *J. Climate*, **5**, 561–576.
- Wang, H., and V. M. Mehta, 2008: Decadal variability of the Indo-Pacific Warm Pool and its association with atmospheric and oceanic variability in the NCEP – NCAR and SODA reanalyses. *J. Climate*, **21**, 5545–5565.
- Wang, H., and M. Ting, 2000: Covariabilities of winter U.S. precipitation and Pacific sea surface temperatures. *J. Climate*, **13**, 3711–3719.
- Wang, H., M. Ting, and M. Ji, 1999: Prediction of seasonal mean United States precipitation based on El Nino sea surface temperatures. *Geophys. Res. Lett.*, **26**, 1341–1344.
- Wilks, D. S., 1995: *Statistical Methods in the Atmospheric Sciences*. Academic Press, pp. 467.
- Williams, C. N., Jr., M. J. Menne, R. S. Vose, and D. R. Easterling, 2007: United States Historical Climatology Network monthly temperature and precipitation data. ORNL/CDIAC-118, NDP-019. [Available on-line at http://cdiac.ornl.gov/epubs/ndp/ushcn/usa_monthly.html].
- Zebiak, S. E., 1993: Air-sea interaction in the equatorial Atlantic region. *J. Climate*, **6**, 1567–1586.

Figure Captions:

Fig. 1. (a) June–August seasonal mean (Unit: mm day^{-1}) and (b) variance (Unit: $\text{mm}^2 \text{day}^{-2}$) of U.S. precipitation based on rainfall data from 1948 to 2007.

Fig. 2. Normalized time series of JJA mean (a) precipitation anomalies averaged over the Southeastern United States ($25^\circ\text{--}36.5^\circ\text{N}$, $76^\circ\text{--}91^\circ\text{W}$) and time series of JJA mean (b) 3-month SPI and (c) 9-month SPI. Black bars in (a) and (b,c) represent wet (positive) and dry (negative) summers with normalized precipitation anomalies and SPI values exceeding 1, respectively, which is indicated by dashed lines. A vertical line divides the two 30-yr periods.

Fig. 3. Percentages of summer days in four rain rate classes. In each category black bar is the 60-year climatological mean and grey bars are the composites of five driest and five wettest summers in the 1948–1977 (light grey) and 1978–2007 (dark grey) periods, respectively. The percentage at the top of each pair of bars indicates the significance level of the composite difference between the two 30-year periods, with F denoting failure of the significance tests, estimated by the Monte Carlo tests with the Bootstrap resampling technique.

Fig. 4. Composites of JJA seasonal mean anomalous (a) 200-hPa height (shading) and zonal wind (contour) and (b) 850-hPa wind (vector), 925-hPa divergence (contour) and U.S. precipitation (shading) associated with one standard deviation of rainfall deficit in the Southeast summer rainfall index. The anomaly fields are obtained based on linear

regressions against the 60-yr Southeast summer precipitation index. Contour intervals are 0.2 m s^{-1} in (a) and 10^{-7} s^{-1} in (b) with negative values dashed and zero contours omitted. Regions of positive (negative) 200-hPa height, zonal wind, and U.S. rainfall anomalies exceeding the 5% significance level are indicated by dark (light) shadings in (c), (d) and (e,f), respectively. Regions of positive (negative) 850-hPa zonal and meridional wind anomalies exceeding the 5% significance level are circled by solid (dash) lines in (e) and (f), respectively.

Fig. 5. Interannual variance of 200-hPa zonal wind anomaly for (a) JJA 1948–1977 and (b) JJA 1978–2007. Values greater than $6 \text{ (m s}^{-1}\text{)}^2$ are shaded and contoured with a contour interval of $2 \text{ (m s}^{-1}\text{)}^2$.

Fig. 6. Homogeneous correlation maps of (a,b) the first SVD mode between Pacific SST and U.S. precipitation, (c,d) the first and (e,f) second SVD modes between Atlantic SST and U.S. precipitation. Correlation coefficients greater than 0.3 are shaded, which exceeds the 5% significance level estimated by the Monte Carlo tests. Positive values of 0.3, 0.5 and 0.7 are also contoured. The dashed-line boxes indicate regions of SST used in the SVD analyses.

Fig. 7. Normalized time series of (a) the first SVD mode between Pacific SST (dark bar) and U.S. precipitation (light bar), (b) the first and (c) second SVD modes between Atlantic SST (dark bar) and U.S. precipitation (light bar).

Fig. 8. Interannual variance of 200-hPa zonal wind anomaly associated with (a,b) the ENSO mode, (c,d) the SST warming trend and (e,f) the Atlantic zonal mode for JJA 1948–1977 (left) and 1978–2007 (right). Values greater than $0.5 \text{ (m s}^{-1}\text{)}^2$ are shaded and contoured with a contour interval of $0.25 \text{ (m s}^{-1}\text{)}^2$.

Fig. 9. Observed (bar) and reconstructed (open square) Southeast summer precipitation index based on multiple linear regressions vs. the time series of the three SVD precipitation modes. Open circle, triangle and closed circle indicate rainfall anomalies associated with individual SVD precipitation modes that are coupled with the ENSO SST, the SST warming trend and the Atlantic zonal mode, respectively.

Fig. 10. Anomaly correlation between hindcasts and observations of precipitation in JJA 1948–2007. Correlation coefficients greater than 0.3 are shaded, which exceeds the 5% significance level estimated by the Monte Carlo tests.

Table 1. Statistics of the three leading SVD modes of SST and precipitation.

	Square covariance	Temporal correlation	SST variance	Precipitation variance
PCF SST–Prec Mode 1	40%	0.63	35%	7%
ATL SST–Prec Mode 1	35%	0.60	23%	10%
ATL SST–Prec Mode 2	19%	0.58	15%	9%

Table 2. Percentages of the total variance in each SVD time series over the two 30 years.

	SST variance 1st 30 yrs	Prcp variance 1st 30 yrs	SST variance 2nd 30 yrs	Prcp variance 2nd 30 yrs
PCF SST–Prcp Mode 1	51%	35%	49%	65%
ATL SST–Prcp Mode 1	35%	39%	65%	61%
ATL SST–Prcp Mode 2	39%	37%	61%	63%

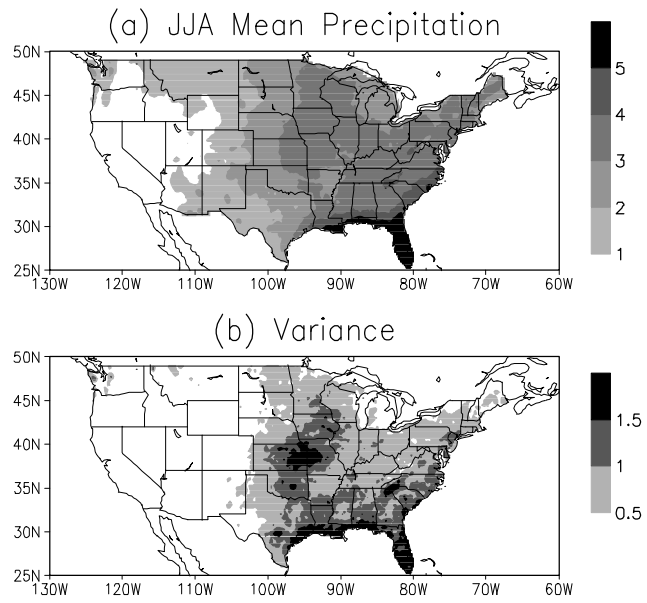


Fig. 1. (a) June–August seasonal mean (Unit: mm day^{-1}) and (b) variance (Unit: $\text{mm}^2 \text{day}^{-2}$) of U.S. precipitation based on rainfall data from 1948 to 2007.

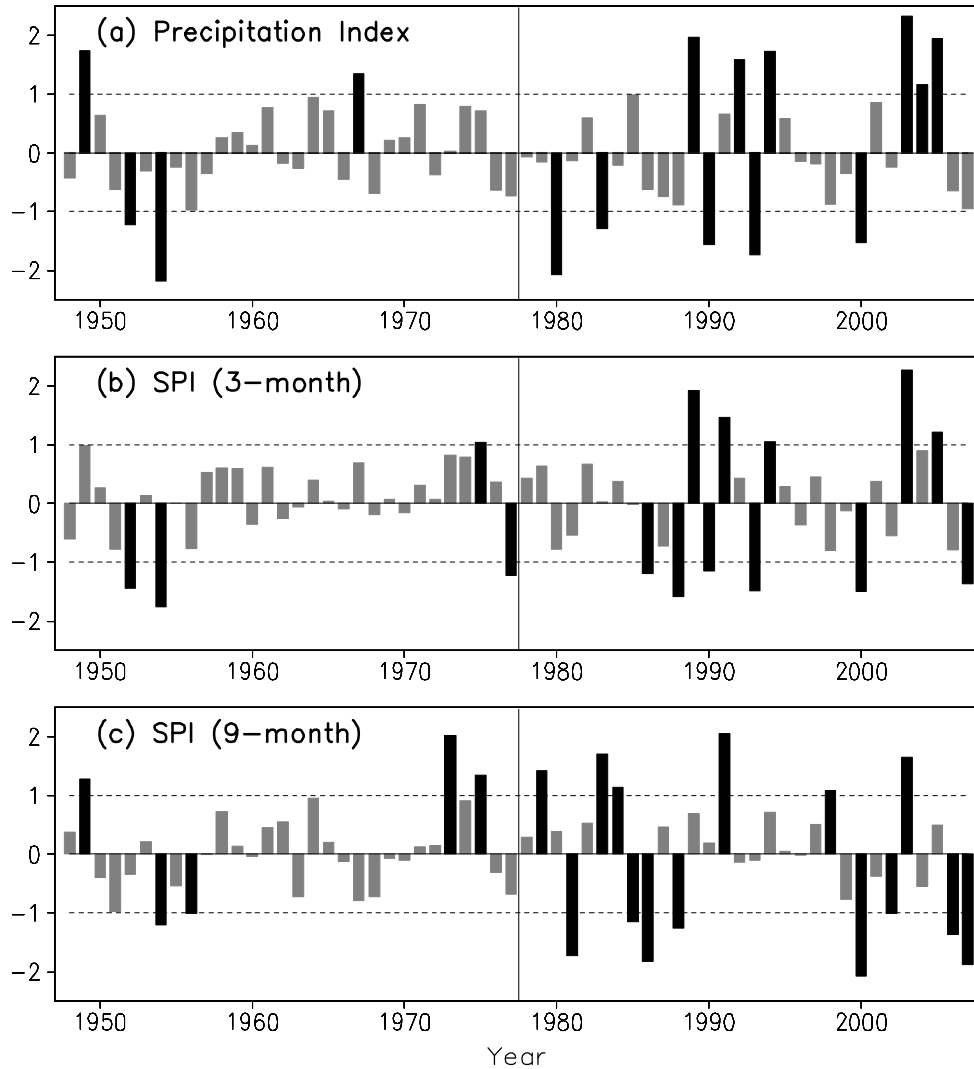


Fig. 2. Normalized time series of JJA mean (a) precipitation anomalies averaged over the Southeastern United States (25° – 36.5° N, 76° – 91° W) and time series of JJA mean (b) 3-month SPI and (c) 9-month SPI. Black bars in (a) and (b,c) represent wet (positive) and dry (negative) summers with normalized precipitation anomalies and SPI values exceeding 1, respectively, which is indicated by dashed lines. A vertical line divides the two 30-yr periods.

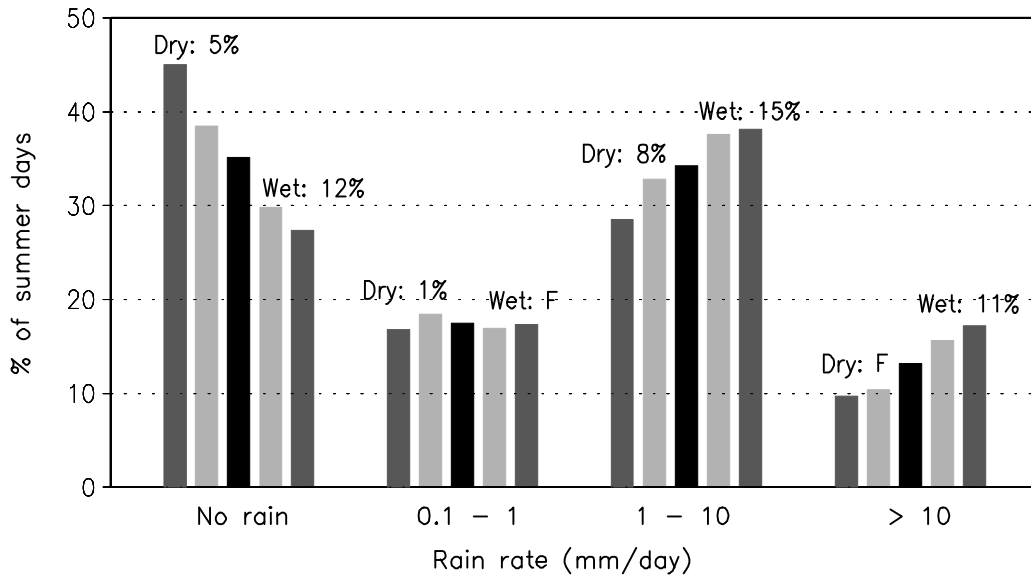


Fig. 3. Percentages of summer days in four rain rate classes. In each category black bar is the 60-year climatological mean and grey bars are the composites of five driest and five wettest summers in the 1948–1977 (light grey) and 1978–2007 (dark grey) periods, respectively. The percentage at the top of each pair of bars indicates the significance level of the composite difference between the two 30-year periods, with F denoting failure of the significance tests, estimated by the Monte Carlo tests with the Bootstrap resampling technique.

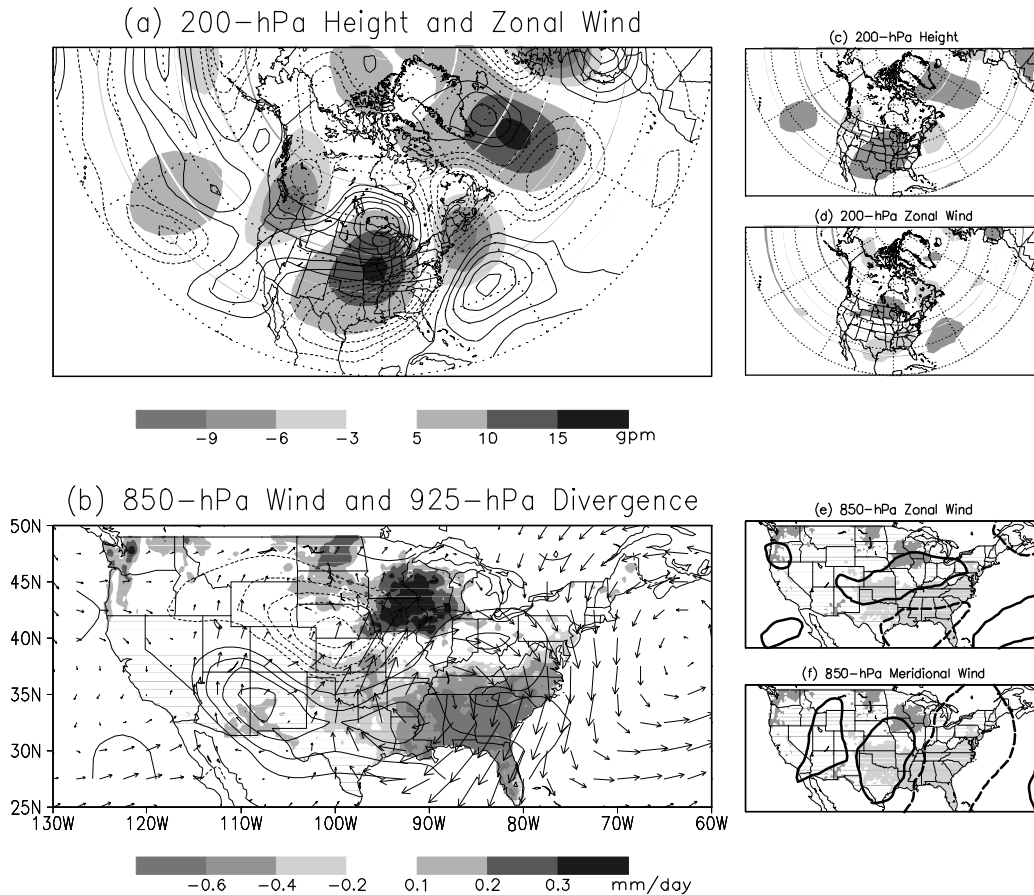


Fig. 4. Composites of JJA seasonal mean anomalous (a) 200-hPa height (shading) and zonal wind (contour) and (b) 850-hPa wind (vector), 925-hPa divergence (contour) and U.S. precipitation (shading) associated with one standard deviation of rainfall deficit in the Southeast summer rainfall index. The anomaly fields are obtained based on linear regressions against the 60-yr Southeast summer precipitation index. Contour intervals are 0.2 m s^{-1} in (a) and 10^{-7} s^{-1} in (b) with negative values dashed and zero contours omitted. Regions of positive (negative) 200-hPa height, zonal wind, and U.S. rainfall anomalies exceeding the 5% significance level are indicated by dark (light) shadings in (c), (d) and (e,f), respectively. Regions of positive (negative) 850-hPa zonal and meridional wind anomalies exceeding the 5% significance level are circled by solid (dash) lines in (e) and (f), respectively.

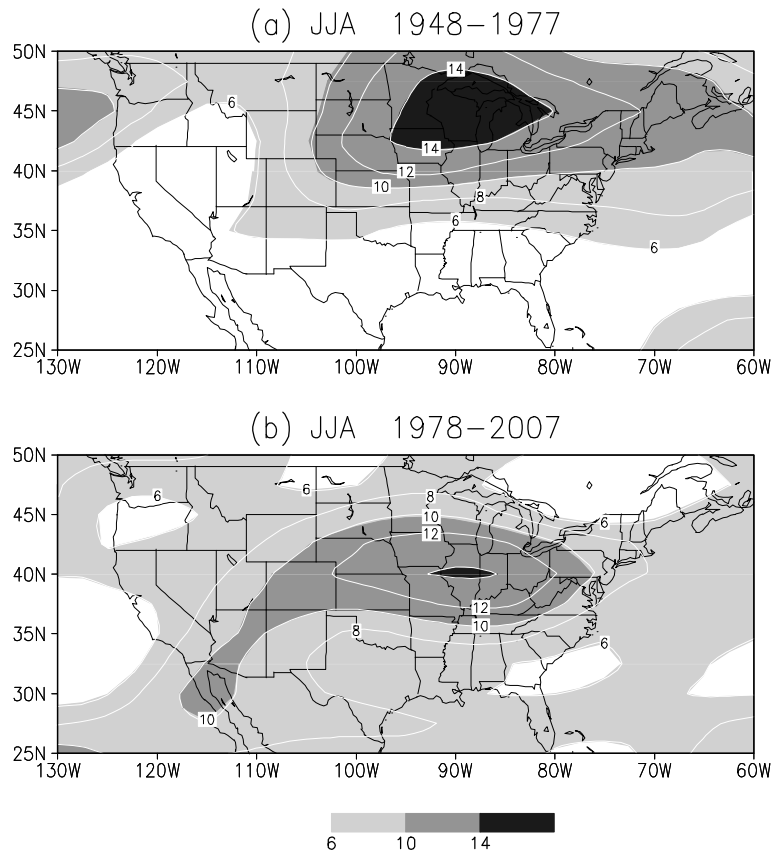


Fig. 5. Interannual variance of 200-hPa zonal wind anomaly for (a) JJA 1948–1977 and (b) JJA 1978–2007. Values greater than $6 \text{ (m s}^{-1}\text{)}^2$ are shaded and contoured with a contour interval of $2 \text{ (m s}^{-1}\text{)}^2$.

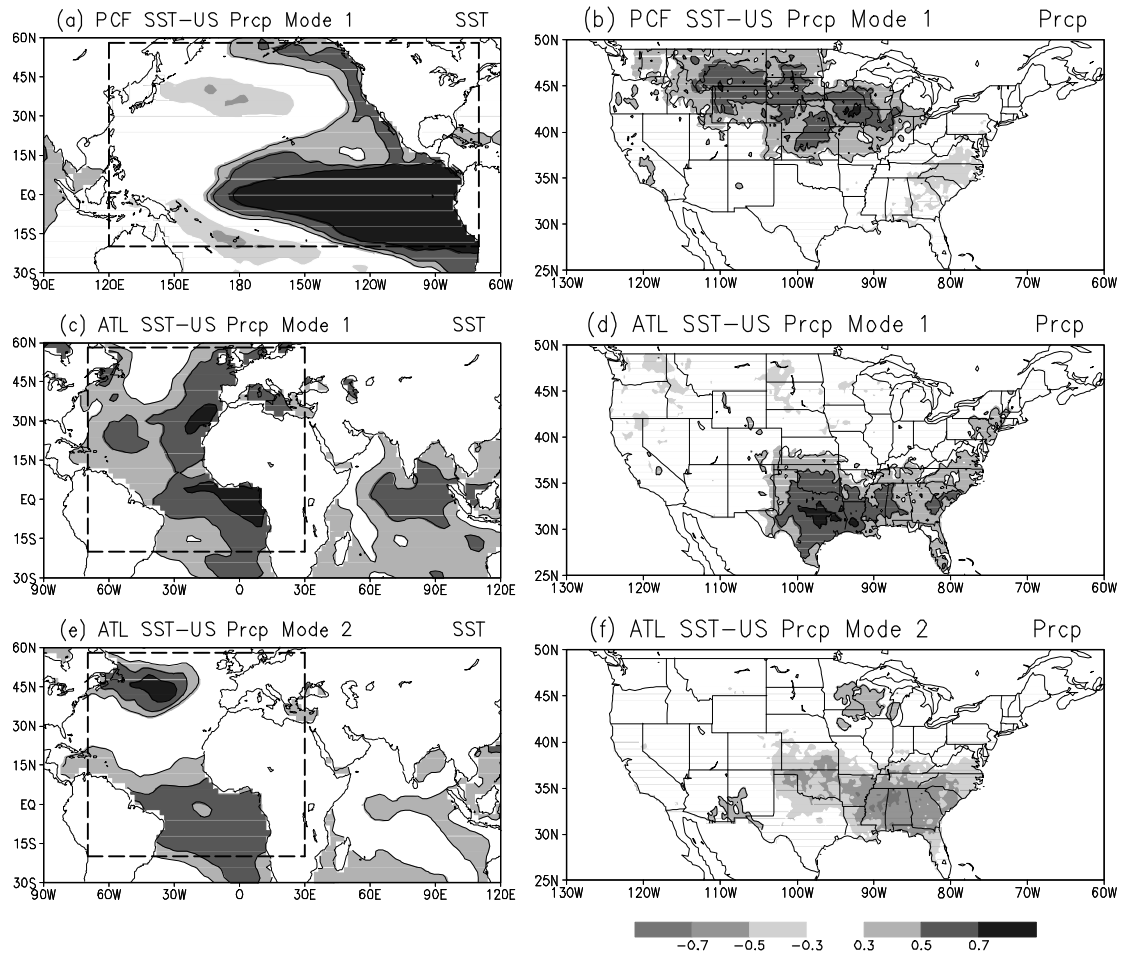


Fig. 6. Homogeneous correlation maps of (a,b) the first SVD mode between Pacific SST and U.S. precipitation, (c,d) the first and (e,f) second SVD modes between Atlantic SST and U.S. precipitation. Correlation coefficients greater than 0.3 are shaded, which exceeds the 5% significance level estimated by the Monte Carlo tests. Positive values of 0.3, 0.5 and 0.7 are also contoured. The dashed-line boxes indicate regions of SST used in the SVD analyses.

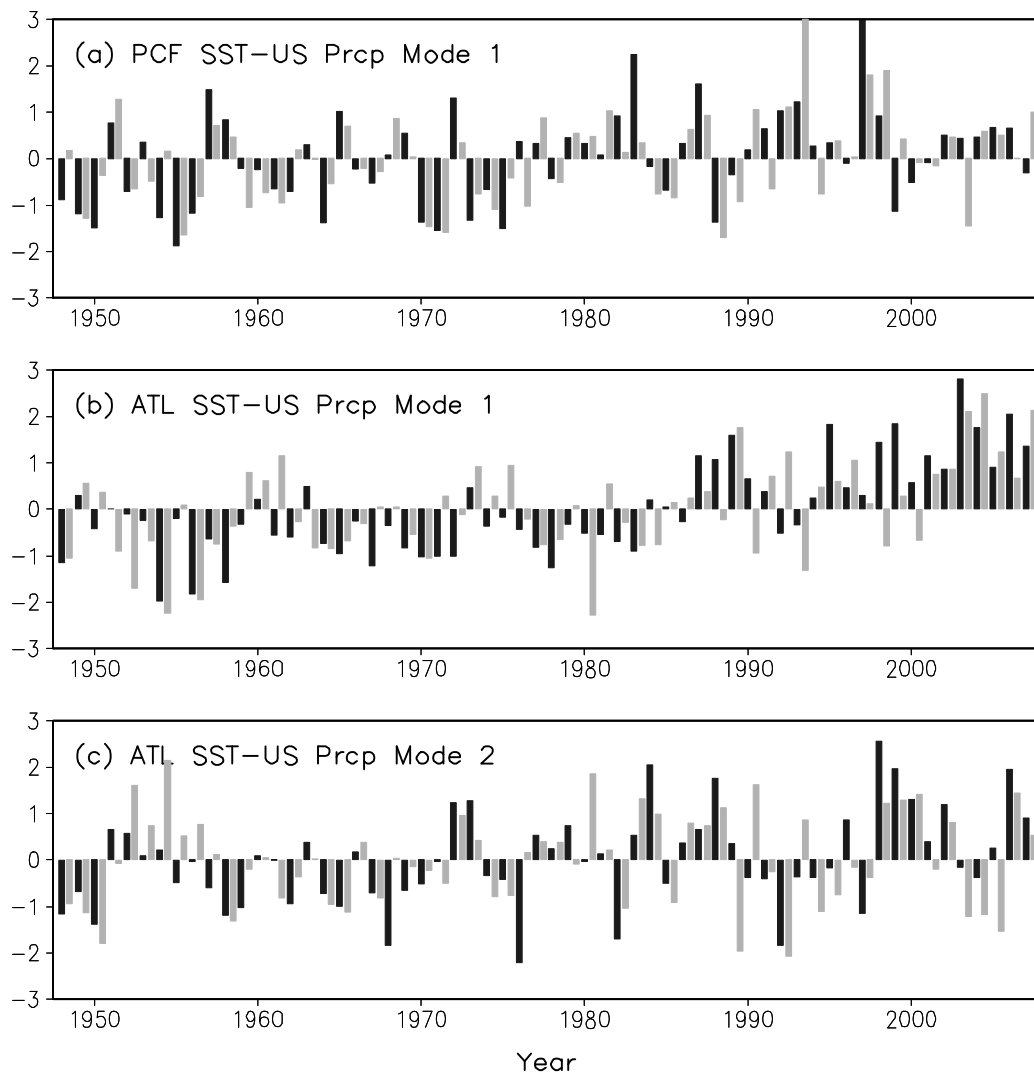


Fig. 7. Normalized time series of (a) the first SVD mode between Pacific SST (dark bar) and U.S. precipitation (light bar), (b) the first and (c) second SVD modes between Atlantic SST (dark bar) and U.S. precipitation (light bar).

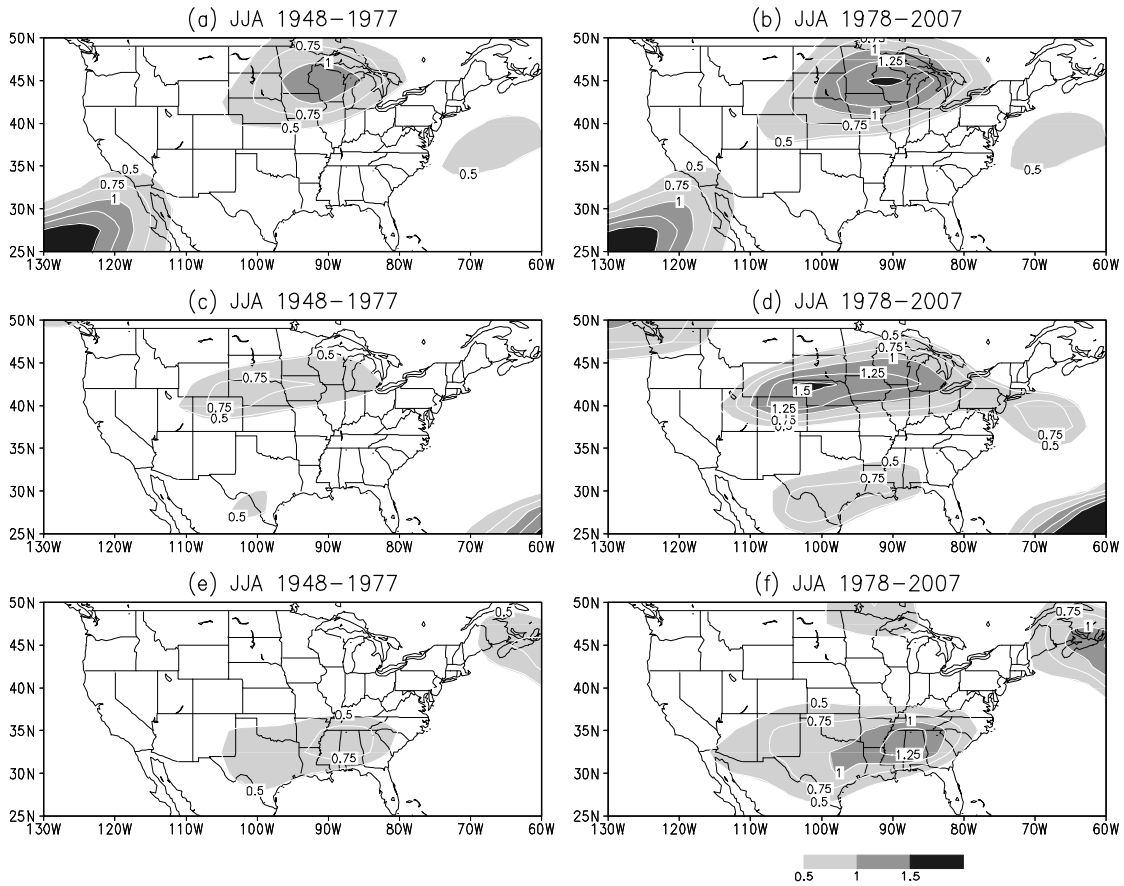


Fig. 8. Interannual variance of 200-hPa zonal wind anomaly associated with (a,b) the ENSO mode, (c,d) the SST warming trend and (e,f) the Atlantic zonal mode for JJA 1948–1977 (left) and 1978–2007 (right). Values greater than $0.5 \text{ (m s}^{-1}\text{)}^2$ are shaded and contoured with a contour interval of $0.25 \text{ (m s}^{-1}\text{)}^2$.

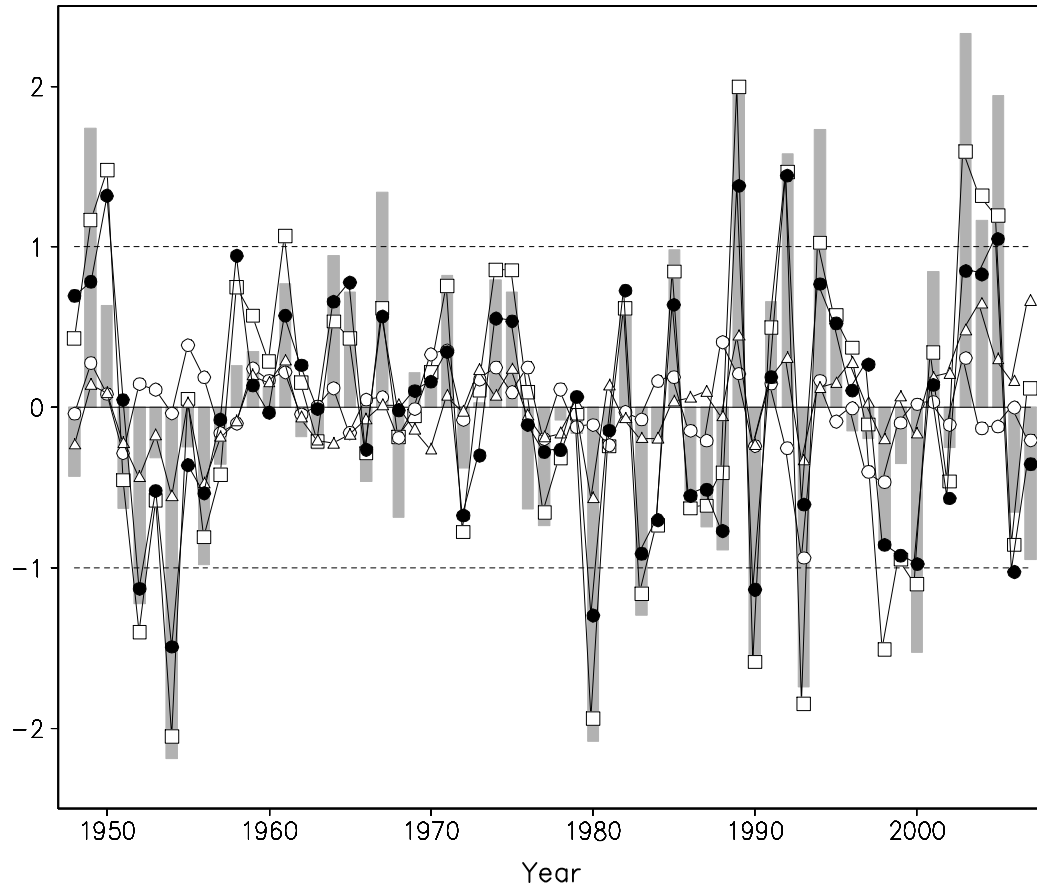


Fig. 9. Observed (bar) and reconstructed (open square) Southeast summer precipitation index based on multiple linear regressions vs. the time series of the three SVD precipitation modes. Open circle, triangle and closed circle indicate rainfall anomalies associated with individual SVD precipitation modes that are coupled with the ENSO SST, the SST warming trend and the Atlantic zonal mode, respectively.

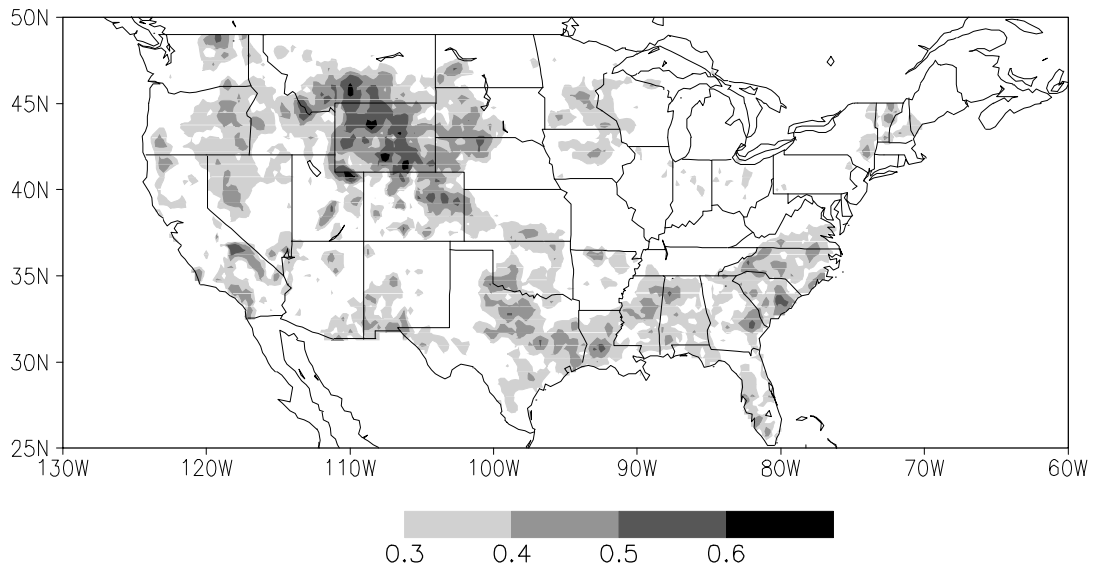


Fig. 10. Anomaly correlation between hindcasts and observations of precipitation in JJA 1948–2007. Correlation coefficients greater than 0.3 are shaded, which exceeds the 5% significance level estimated by the Monte Carlo tests.